AIAA JOURNAL
Vol. 43, No. 5, May 2005

Reduced-Order Structure of Reacting Rectangular Jets

Jennifer L. Edwards* and Frederick C. Gouldin†
Cornell University, Ithaca, New York 14853
and
Fernando F. Grinstein‡ and Kazhikathra Kailasanath§
U.S. Naval Research Laboratory, Washington, D.C. 20375

The results of proper orthogonal decomposition analyses on CO_2 number density and vorticity magnitude data from reacting rectangular jet simulations are presented. The resulting proper orthogonal decomposition eigenfunctions are used to develop physical insight of the vortex formations and dynamics of these jets and their related mixing and spreading characteristics. It is seen that different vortex structures are captured in the eigenfunctions and that CO_2 and vorticity eigenfunctions are very similar indicating that vortex-driven mixing dominates in these jets. The eigenvalue spectra associated with these eigenfunctions are used to evaluate the information content of the eigenfunctions and the potential for reduced-order models. Using subsets of eigenfunctions with high information content, CO_2 and vorticity magnitude distributions can be represented with relatively few eigenfunctions. However, as the flows develop downstream, more eigenfunctions are needed to represent them to the same level of accuracy. The potential for reduced-order modeling of each field is approximately the same for the jets of aspect ratios 1, 2, and 3; however, there is stronger potential for reduced-order modeling of the CO_2 field than of the vorticity field.

Nomenclature

$\boldsymbol{A}$	=	matrix of time coefficients
AR	=	jet aspect ratio
$\boldsymbol{a}_i$	=	column vector of associated time coefficients in $\boldsymbol{A}$ determined via proper orthogonal decomposition (POD)
$\boldsymbol{C}$	=	matrix containing the ensemble of distributions
$\boldsymbol{D}$	=	two-time correlation matrix
De	=	circular-equivalent jet diameter
dx	=	cell spacing of output grid
E_M	=	amount of information contained in M eigenfunctions
e_{abs}	=	normalized absolute error between two distributions
e_{rms}	=	normalized root mean square error between two distributions
f	=	Strouhal frequency of jet forcing
$\boldsymbol{G}$	=	integration matrix
$\boldsymbol{I}$	=	identity matrix
M	=	number of eigenfunctions used in the representation
N_m	=	number of eigenfunctions used in the expansion
N_p	=	total number of spatial points
N_t	=	total number of time realizations
N_x	=	number of grid points in the x direction
N_z	=	number of grid points in the z direction
n	=	scalar distribution of vorticity magnitude or concentration (number density—molecules/cm^3)
$\hat{n}$	=	best representation of a scalar distribution
Sr	=	Strouhal number of jet exit flow
t_k	=	kth time step in the large-eddy simulation
Uo	=	jet-exit velocity
x, z	=	Cartesian coordinates in the cross-stream direction
y	=	Cartesian coordinate in the axial direction
y_0	=	transitional location
β_i	=	associated eigenfunction weighting factor for best representation
Δ	=	grid cell size
θ	=	initial momentum thickness
$\boldsymbol{\Lambda}$	=	matrix of eigenvalues
λ_i	=	ith eigenvalue
$\bar{\lambda}_i$	=	normalized ith eigenvalue
$\boldsymbol{\Phi}$	=	matrix of POD eigenfunctions
ϕ_i	=	row vector of the ith POD eigenfunction in $\boldsymbol{\Phi}$
$\Omega_{\max}$	=	maximum value of vorticity magnitude

Presented as Paper 2002-1011 at the 40th Aerospace Sciences Meeting, Reno, NV, 14–17 January 2002; received 24 November 2003; revision received 7 December 2004; accepted for publication 13 December 2004.

*Graduate Student, Sibley School of Mechanical and Aerospace Engineering, Upson Hall. Member AIAA.
†Professor, Sibley School of Mechanical and Aerospace Engineering. Associate Fellow AIAA.
‡Research Physicist, Laboratory for Computational Physics and Fluid Dynamics. Associate Fellow AIAA.
§Head, Center for Reactive Flow and Dynamical Systems, Code 6410. Fellow AIAA.

Introduction

COMBUSTION control technologies are under development for application to advanced combustion and propulsion systems.[1–13] Detection and control of the large-scale flow and scalar features in these systems are of primary importance as internal mixing control can improve combustor performance.[1,2,6,10,14] An overview of combustion dynamics and control can be found in the review article by Candel.[8] The behavior of a combustion system is governed by a set of partial differential equations (PDEs) that describe the fluid dynamics, combustion dynamics, heat transfer, and acoustics of the system.[15] These PDEs and their associated boundary conditions define a system state located in an infinite-dimensional state space[16–18] that can change as a function of both time and condition. Detailed solution of the PDEs is impractical for control applications, and finite-dimensional or reduced-order models become necessary to describe the behavior of the system. Reduced-order models representing the dynamics of a combustion system are crucial to the development of effective combustion control, by providing a model of the system and how it responds to control actuation.[3,4,8,9,11] For control applications, these models have been developed in two ways: 1) through projection of the governing equations onto a subspace defined by a chosen basis set[18–21] and 2) through a system identification approach where a mathematical model describing the relationships among the important system variables is obtained from empirical input and output data, often including expansions of individual input or output parameters in a basis set.[11,22] It has been shown that the performance of a control system depends highly on the quality of the basis set used,[19] and proper orthogonal decomposition eigenfunctions

are often utilized[9,11,19,21,23–25] because of their ability to represent important parameters efficiently, requiring only a small number of eigenfunctions in an expansion.

The Karhunen–Loeve (KL) procedure, or proper orthogonal decomposition (POD), is one method that could be used to develop reduced-order models and investigate large-scale structures of a combustion system. POD decomposes a set of distributions or functions, the ensemble, into an optimal orthonormal set of eigenfunctions able to represent the distributions of the ensemble.[18,26–28] These distributions are represented as a weighted expansion of the eigenfunctions. Subsets of these eigenfunctions can offer highly efficient representations of important variables in combustion systems. They are optimal in the sense that they contain the most information relative to any other basis set and allow one to capture the dominant features of a system using the fewest basis functions in an expansion. Examination of a few POD eigenfunctions quickly identifies the most important large-scale structures of the flow enabling the researcher to visualize the flow behavior and determine where more detailed investigation is desired. Furthermore, the potential for a reduced-order model utilizing these basis functions can be evaluated from their information content as determined from the associated eigenvalue spectrum derived from POD. The eigenvalue spectrum quantifies the average contribution of each eigenfunction in representing the distributions in the ensemble, and thus its relative importance, to the representation of the system properties. For a reduced-order model utilizing an expansion in a set of basis functions, a measure of the potential for modeling is the number of basis functions necessary to capture the flow physics. Because the POD eigenfunctions provide an optimal basis set, the number of POD derived basis functions required will be the lowest of any basis set, and POD analysis can be used as a best case to evaluate the potential for modeling.

Proposed by Lumley in 1967 as a method to recover coherent structures in turbulent flows,[29] POD has become widely used for investigation of organized structures in jet flows. POD has been used to study velocity data generated by numerical simulation[30,31] as well as particle image velocimetry[32,33] and hot-wire measurements[34–36] in various jet configurations. POD has also been applied to scalar fields such as concentration and temperature produced by numerical simulation[30,31,37] and experimental measurement.[32,38,39] POD has been used by a number of researchers to study various spatial structures in physical flows and systems[18,26,27]; for example, it has been applied to the study of turbulent mixing in jets[40] and facial pattern recognition.[27] POD results are frequently used to study the dynamics and understand the nature of jet flows. For instance, results have been used to examine the stagnation-point location and radial velocity fluctuations in an annular jet.[33] The relation between jet stability and jet flapping and penetration were examined for a round jet in a counterflow,[32] and vortex rings and jet flapping were investigated in round jet-like flows.[39] POD results are also commonly applied to the identification and evolution of large-scale structures in jet flows and used in low-dimensional representations of the fields studied.[31,34–38] Tornianen et al. developed a tomographic reconstruction technique using POD eigenfunctions as basis functions, taking advantage of the optimality of the eigenfunction set and the ability to represent a scalar field using relatively few basis functions.[37]

Low-dimensional models based on Galerkin projection of the governing equations onto POD eigenfunctions have been developed.[9,11,30,41,42] Studies have utilized POD eigenfunctions to develop reduced-order models of flow over compliant wall surfaces and coherent structures in turbulent boundary layers[41] as well as turbulent plane Couette flow.[42] Models based on POD eigenfunctions have been developed to describe burning characteristics and instability in combustion systems for use in control applications.[9,11] POD eigenfunctions have also been used with partial measurements of data fields in a H_2/air opposed-jet diffusion flame to estimate "unmeasured" quantities, showing that POD eigenfunctions have good interpolative properties.[31] The forced one-dimensional turbulent jet studies of Faghani et al. showed that eigenfunctions depend on the domain of measurements but are possibly invariant in a given flow for certain relevant parameters, for example, Reynolds number.[35] It has been suggested that the use of POD eigenfunctions can be extended to situations similar to that from which they were derived if the ensemble of distributions from which the eigenfunctions were generated is sufficiently large and contains sufficient information on the dynamics of the system.[20,35] However, for the majority of applications, models utilizing POD eigenfunctions are developed for a specific system. Because of the need for an ensemble of distributions, the eigenfunctions must be derived from computational[9,19,21,23,24] or experimental data[11,23,25] representative of the system of interest and are sometimes referred to as empirical eigenfunctions. The necessary ensemble can contain distributions resulting from various operating states of a system or a set of measured or simulated time realizations of important variables in an unsteady process.

The majority of the studies just mentioned were applied to axisymmetric or plane jets. The studies were performed on nonforced and forced[35–37] flows, and, with the exception of Refs. 31 and 37, the jet studies were performed on nonreacting flows. Forced jets are of particular interest because of their use as actuators in combustion control applications.[3–7] Rectangular jets have been shown to passively improve mixing of the jet (e.g., fuel) with its surroundings (oxidizer) through enhanced entrainment as a result of axis switching and to enhance mixing near corner regions and far downstream.[1,43–45] Entrainment and mixing control are highly dependent upon the development of large-scale coherent vortical structures in the flow and their breakdown into turbulence.

We are investigating CO_2 and vorticity magnitude data in forced rectangular reacting jets of varying aspect ratios as nonpremixed flames where fuel-oxidizer mixing is required for chemical reaction.[43,44] Near the jet exit, CO_2 production is governed primarily by fuel-air mixing through the vortex formations there, whereas farther downstream, its presence is governed not only by production in mixed zones, but also by convective and diffusive transport. CO_2 concentration data are useful as an indicator of overall mixing, as well as being an important measure of combustion progress. Vorticity magnitude data are investigated because of the importance that vorticity plays in the mixing and entrainment of these jets and the connection between combustion instabilities and vortex dynamics.[10,14,46]

Data for the jet flows studied are obtained from large-eddy simulation (LES) of the jets, reported separately.[43,44] Although both experimental and numerical simulation data can be used for the POD analysis, the need for a large number of distributions in the ensemble makes simulation data the most attractive choice. LES reduces the need for the extensive computational resources required by direct numerical simulation (DNS) and eliminates the need for experimental resources needed to gather large amounts of data on multiple jets for this study.

In this paper the results of POD applied to CO_2 concentration and vorticity magnitude fields in forced rectangular reacting jets of aspect ratios $AR = 1$–3 are reported and discussed. By consideration of eigenvalue spectra and eigenfunction information content, we evaluate the potential for reduced-order modeling of vorticity and scalar fields in forced rectangular jets using a limited number of basis functions. In addition, we investigate the structures of these jets through the study of the vorticity magnitude and CO_2 concentration fields. Through comparison of these two fields, we can investigate the effect of vorticity on jet mixing and combustion and extract physical insight about the jet structures.

Reacting Rectangular Jets

LES of turbulent reacting rectangular jets was performed on forced jets of varying aspect ratios ($AR = 1$–3).[43,44] Monotonically integrated LES (MILES)[43–45,47–52] was used for the LES computations in this paper. The MILES approach involves solving the unfiltered Euler or Navier–Stokes equations with high-resolution, locally monotonic algorithms such as the flux-corrected-transport (FCT) method or the piecewise parabolic method. Nonlinear high-frequency filters built into the algorithms provide implicit subgrid-scale (SGS) models eliminating the use of explicit SGS models introduced for closure in conventional LES. Formal properties of the effectual SGS modeling using MILES are presented in Refs. 44 and 48.

By design, the simulated rectangular jets differed in *AR* but had otherwise essentially identical initial conditions, including nearly identical *De*. Propane–nitrogen jets were issued into a quiescent oxygen–nitrogen background, with reactant molar concentrations chosen to be the same and equal to 0.4, a Mach number of 0.3, and Reynolds number greater than 8.5×10^4—based on the jet-exit velocity Uo and the circular-equivalent jet diameter De (the diameter of a round jet having the same cross-sectional area). Typical Reynolds number for the jets discussed in this paper is $Re = UoDe/\nu > 8.5 \times 10^4$ based on estimated upper bounds for the effective numerical viscosity of the FCT algorithm.[44,49] The jets were initialized with laminar conditions, thin rectangular vortex sheets, slightly rounded-off corner regions, and uniform initial momentum thickness θ, such that $De/\theta = 50$. The jet-exit velocity was forced axially by superimposing a single-frequency sinusoidal perturbation on the jet-exit velocity, $Uo = 200$ m/s, having an rms level of 2.5% and Strouhal frequency $Sr = fDe/Uo = 0.48$.

A global (single-step irreversible) model for propane chemistry was used,[44,53] $C_3H_8 + 5O_2 \rightarrow 3CO_2 + 4H_2O$, with the fuel consumption rate given by $\omega = A_r \exp(-E_{\text{act}}/RT)[C_3H_8]^{\alpha}[O_2]^{\beta}$, $\alpha = 0.1$, $\beta = 1.65$, $A_r = 8.6 \times 1011$ $\text{cm}^{2.25}\text{mol}^{-0.75}\text{s}$, and $E_{\text{act}} = 30$ kcal mol^{-1}. As the fuel consumption rate is sensitive to fuel and oxidizer concentrations as well as temperature, it can handle extinction and reignition in a limited manner when there are large fluctuations in concentrations or temperature. Given the simplified chemistry model used and the assumption of near unity Lewis numbers (typical *Le* range from 0.8 to 0.94), coupling relations between species and temperature can be developed.[54,55] With these assumptions, it is expected that temperature or species data for the POD analysis will provide the same information with regard to the potential for modeling of these fields. Convective mixing (stirring) and fast chemistry dominate in the flow regime of these jets (fast flow, high Damkohler number), such that this combustion model is useful to provide a reasonable, simple framework to assess the utility of POD. This chemistry model is reasonable for calculating heat-release rate for use in combustion instability and control studies.[47,50] The background gases were at 1400 K to ensure autoignition of the jet. Multispecies temperature-dependent diffusion and thermal conduction processes were calculated explicitly using central difference approximations and coupled to the chemical kinetics and convection using time-step-splitting techniques. The numerical model was second order in space and time.[47] Subgrid fluctuations were neglected, and instantaneous evaluation of relevant combustion quantities such as diffusivities, thermal conductivities, and fuel burning rates was performed directly in terms of unfiltered variables. Further details on the simulated transport properties and their validation are discussed in Refs. 43, 44, and 47 and references therein.

The close relationship between unsteady fluid dynamics and nonpremixed combustion in high-speed propane jets emerging into an air background was used to illustrate the potential practical impact of the vortex dynamics on the jet entrainment. For the jet regimes considered, large-scale vortex-driven convective mixing dominated, and instantaneous entrainment and fuel-burning rates were highly correlated.[47] These are precisely the kinds of regimes (large-scale driven entrainment, mixing, and combustion) where LES can be expected to be useful. Moreover, because the regimes involve near-unity jet-to-background density ratio and virtually negligible preferential diffusion effects such that differences in Lewis and Schmidt numbers between the jet and surroundings are small, the results for propane reactive jets discussed are not very dependent on the combustion specifics.[44,47] The main focus of the simulations is to relate unsteady jet combustion and fluid dynamics while examining the basic topological features of the jets.

Jet simulations were performed on a $140 \times 200 \times 140$ computational grid, and the results were presented on a $120 \times 200 \times 120$ inner subdomain, at up to 63 equally spaced times with time interval $= 0.1/f$. The cell spacing dx of the output grid was equal to 0.015 cm, and the reference equivalent jet diameter was $De = 0.338$ cm (Fig. 1). Jet dimensions are 0.3×0.3, 0.21×0.42, and 0.18×0.54 cm for the $AR = 1$, 2, and 3 jets, respectively. Convergence studies indicate that the MILES approach is capable of capturing the dominant inertial subrange in these flows. Previous spectral analysis[45] of the jets presented on the coarse and fine grids in Appendix A showed similar trends for amplitudes and self-similar behaviors on the smallest resolved scale. Grid-resolution issues in the context of POD are addressed in Appendix A.

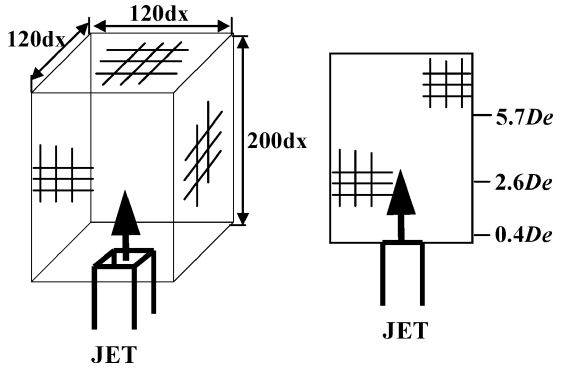

Fig. 1 Schematic diagram of computational domain representing the output grid provided for this study.[37]

Proper Orthogonal Decomposition

Proper orthogonal decomposition is a mathematical procedure that we have applied to the study of reacting forced jets. It is useful because it produces an optimal orthonormal set of eigenfunctions from an ensemble of distributions. The eigenfunctions are optimal in the sense that they are calculated to have the smallest mean-squared error in representing the ensemble of distributions for any fixed number of terms in the expansion compared to any other basis set.[26–28] Because of the optimality of the POD basis set, it can be used as a best case to evaluate the potential for development of a reduced-order model utilizing an expansion in any set of basis functions, making POD analysis useful to the development of reduced-order models of the system under investigation. POD is used here to investigate the potential for reduced-order modeling of forced reacting rectangular jet systems through evaluation of the eigenvalue spectra and eigenfunction information content, as well as to capture and study large-scale features of these jet flows, specifically large-scale spatial structures in CO_2 concentration distributions and vorticity magnitude distributions. The most important POD eigenfunctions contain those structures that are the most significant, primarily large-scale structures. Because the large scales are well resolved with LES and we are interested in retaining the most important eigenfunctions for modeling and analysis, POD analysis is well suited for this study. Information regarding the spatiotemporal behavior of the large-scale structures can be gained from the results of POD applied to the CO_2 and vorticity fields.

An ensemble of time realizations such as those in this study can be expanded as a superposition of KL eigenfunctions, each with a set of associated time coefficients that correspond to all of the time realizations of the ensemble. Each eigenfunction also has an associated eigenvalue, which classifies the importance of the eigenfunction to the representation of the ensemble of time realizations. The eigenvalues are the mean square of the associated time coefficients. The KL eigenfunctions and time coefficients are determined from a matrix eigenvalue problem via the method of snapshots.[27,28] Using this method, eigenfunctions are given by a superposition of instantaneous distributions from the set of time realizations, producing an intrinsically defined basis set. Details of formulation of the matrix problem that follows are included in Appendix B.

Two-dimensional POD decomposes the ensemble of scalar distributions $\{n\}$, calculated at a set of discrete time realizations (t_k) and chosen at specified axial locations in the jet, into a set of eigenfunctions $\{\phi\}$ with time coefficients $\{a\}$:

$$n(x_i, z_j, t_k) = \sum_{l=1}^{N_m} a_l(t_k)\phi_l(x_i, z_j)$$

$$i = 1, \ldots, N_x, \qquad j = 1, \ldots, N_z, \qquad k = 1, \ldots, N_t \quad (1)$$

N_x and N_z are the number of grid points in the x and z directions, respectively, equal to 120 in both directions, N_t is the number of time realizations analyzed (approximately 60), and N_m is the number of eigenfunctions used in the expansion.[27,28,37] Generally, the number of eigenfunctions N_m necessary for a sufficient representation of a distribution $n(x, z, t_k)$ is much smaller than the total number of eigenfunctions provided by the POD analysis N_t.

As noted, the eigenfunctions are given by a superposition of instantaneous distributions producing an intrinsically defined basis set. The time coefficients and eigenfunctions are calculated by solving the following matrix eigenvalue problem through Cholesky factorization:

$$\boldsymbol{DA} = \boldsymbol{A\Lambda} \tag{2}$$

where $\boldsymbol{D} \in \boldsymbol{R}^{Nt \times Nt}$, $\boldsymbol{A} \in \boldsymbol{R}^{Nt \times Nt}$, and $\boldsymbol{\Lambda} \in \boldsymbol{R}^{Nt \times Nt}$. $\boldsymbol{\Lambda}$ is a diagonal matrix containing the associated eigenvalues.[27,28,37] The two-time correlation matrix $\boldsymbol{D}$ is defined by

$$\boldsymbol{D} = (1/N_t)\boldsymbol{CGC}^T \tag{3}$$

where $\boldsymbol{C}$ is a $N_t \times N_p$ ($N_p = N_x \times N_z$) matrix containing the ensemble of distributions and $\boldsymbol{G}$ is a $N_p \times N_p$ integration matrix. The integration matrix $\boldsymbol{G}$ is used to obtain the discrete estimate of the two-time correlation matrix $\boldsymbol{D}$ (Ref. 28). The eigenfunctions are then calculated as[28,37]

$$\boldsymbol{\Phi} = (1/N_t)\Lambda^{-1}A^T\boldsymbol{C} \tag{4}$$

where the $N_t \times N_p$ matrix $\boldsymbol{\Phi}$ contains N_t eigenfunctions that are normalized according to

$$\boldsymbol{\Phi G \Phi}^T = \boldsymbol{I} \tag{5}$$

The eigenvalue λ_i, associated with the eigenfunction ϕ_i, classifies the importance of that eigenfunction in the representation of the ensemble of distributions investigated. The eigenfunctions are arranged in order of importance, the first eigenfunction having the largest eigenvalue and the last eigenfunction having the smallest eigenvalue. The total amount of information present in a subset of eigenfunctions, termed the information content, can be evaluated as the sum of the subset of normalized eigenvalues. It is therefore possible to estimate the contribution of any particular eigenfunction or subset of eigenfunctions to a representation by determining the information content therein [see Eq. (7)]. It is important to note, however, that the "importance" of an eigenfunction to the representation is an average quantity of the entire ensemble and may be described as an ensemble average importance. However, for any given distribution in the ensemble, the amount of information a particular eigenfunction can capture in the distribution can differ from the amount of information it captures in the ensemble on average.

For this study, the eigenvalues were normalized as

$$\bar{\lambda}_i = \lambda_i \Big/ \sum_{j=1}^{N_m} \lambda_j \tag{6}$$

following the analysis in Ref. 37 and were used to classify the information content of a subset of the first M eigenfunctions E_M (sometimes referred to as the "energy" of an eigenfunction[26,27])

$$E_M = \sum_{i=1}^{M} \bar{\lambda}_i \tag{7}$$

Results

POD is used here to investigate the potential for reduced-order modeling of forced reacting rectangular jet systems through analysis of eigenfunction information content, as well as to capture large-scale spatial structures in concentration and vorticity magnitude distributions. Information regarding the spatiotemporal behavior of the large-scale structures is investigated using the results of POD applied to these fields. Results were obtained by performing POD on sets of planar CO_2 concentration and vorticity magnitude distributions containing approximately 60 time realizations. Distributions at seven axial locations were examined: $y = 0.4De$, $2.2De$, $2.6De$, $3.3De$, $4.8De$, $5.7De$, and $6.6De$. Results representative of the CO_2 and vorticity fields are presented here for $y = 0.4De$, $2.6De$, and $5.7De$.

CO_2 Concentration

The first KL eigenfunctions of CO_2 concentration are presented in Fig. 2 for the axial locations just described in reacting rectangular jets of aspect ratios 1–3. The normalized eigenvalue spectra corresponding to the eigenfunctions produced by POD at these locations are shown in Fig. 3. The first eigenfunction, having the largest eigenvalue, is considered to be the eigenfunction most closely correlated to the distributions contained in the ensemble and the single eigenfunction that best represents the jet distributions.[37] This eigenfunction contains over 95% of the total information in the set of eigenfunctions at $0.4De$ and over 75% of the information at $5.7De$ for the aspect ratios considered; see Table 1. Close to the jet exit (at $0.4De$), the first eigenfunction for each jet shows some lobes beginning to develop near the corner regions of the jets. In the center of each eigenfunction is a rectangular region where no CO_2 is present, indicating the fuel region of the jet. At locations close to the jet exit, the first eigenfunctions are of similar shape for each aspect-ratio jet. However, farther downstream (at $2.6De$), the eigenfunctions begin to differ as a result of different vortex dynamics between the jets.[43,44] Lobes develop at the corners of each jet; however, these lobes are far more pronounced for $AR = 1$ than for $AR = 2$ or 3. The lobes increase the spreading of the square jet in the corner regions over that of the rectangular jets at this axial location. For aspect ratios of 2 and 3, ridges develop along the major sides of the rectangular jets that are less prominent in the case of the square jet. The peak levels of CO_2 are approximately the same in the eigenfunctions for the different aspect ratios, consistent with the results from numerical simulations of these jets.

Far downstream (at $5.7De$), the first CO_2 eigenfunctions are much more diffuse and complex. The lobes and ridges that are well defined at $y = 2.6De$ have lost their definition and become more random. The eigenfunctions suggest better mixing and entrainment in the $AR = 2$ and especially $AR = 3$ jets compared to the square jet. This is evident in the more uniform concentration of the first eigenfunctions in the rectangular jets when compared to the square case and is caused by more intense streamwise vorticity in these jets.[43,44] More extensive spreading of the CO_2 field in the $AR = 3$ and, to some extent, the $AR = 2$ jets is also noted at this axial location, in contrast to axial locations closer to the jet exit where there is enhanced spreading of the square jet. Note that the fuel core region remains visible even at these downstream locations.

Vorticity Magnitude

The first eigenfunctions of vorticity magnitude are displayed in Fig. 4 for axial locations $y = 0.4De$, $2.6De$, and $5.7De$ with the corresponding normalized eigenvalue spectra for these locations displayed in Fig. 3. The second eigenfunctions of vorticity are displayed in Fig. 5. Eigenfunction information content is presented in Table 1.

The eigenfunctions display well-defined vortex structures at $y = 0.4De$ and $2.6De$. Vorticity magnitude data after vortex structure breakdown and transition to turbulence in the far jet are displayed at $5.7De$. The vorticity eigenfunctions also capture different vortex structures in the flow dependent on the aspect ratio of the jet. The structures apparent in the corresponding eigenfunctions of $AR = 2$ and 3 jets are similar to each other; however, different vortex structures are apparent in the corresponding eigenfunctions of the square jet. This reflects the inherent differences in the vortex dynamics of square vs rectangular jets. Although different vortex structures can be captured in the eigenfunctions of the three jets, eigenvalue spectra suggest that the same number of eigenfunctions for each of the jets is required to capture a specified amount of information in the flow.

Although the vorticity magnitude does not contain any directional information, previous studies have determined the dynamics

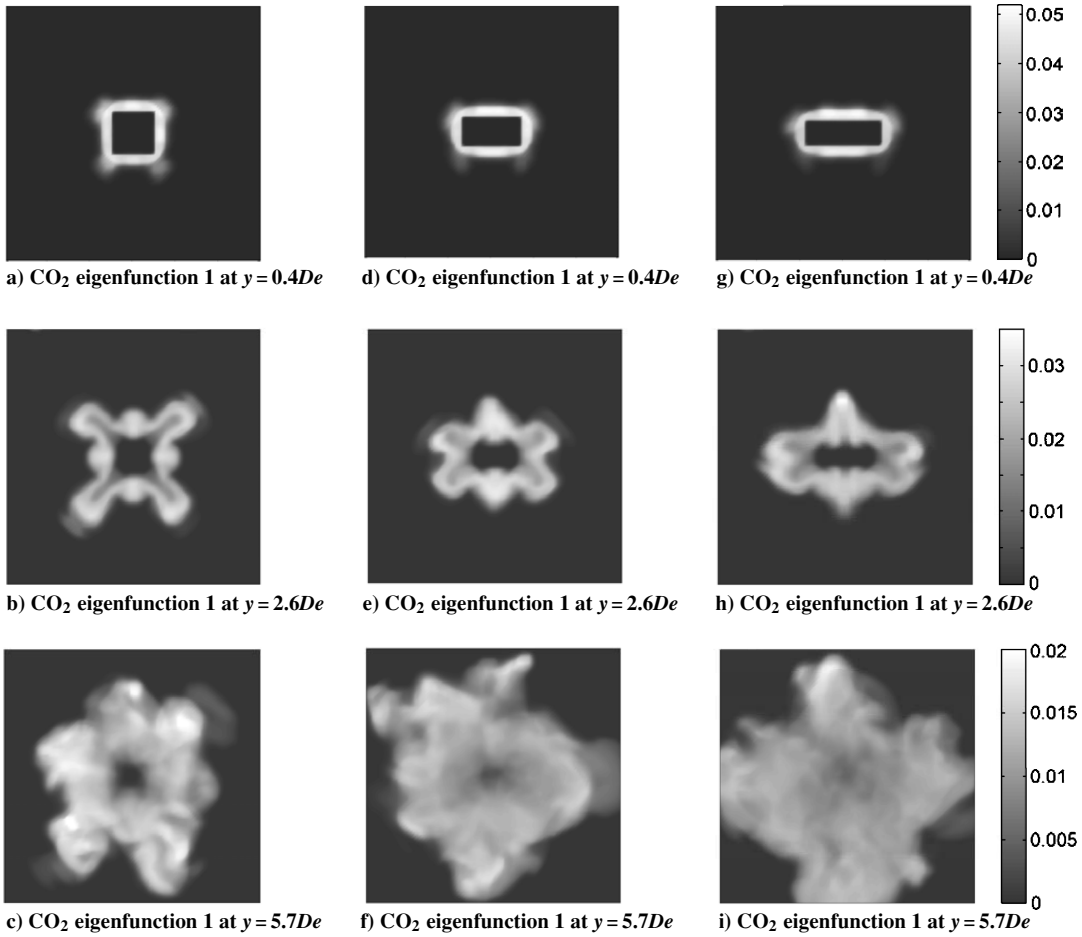

a) CO_2 eigenfunction 1 at $y = 0.4De$ d) CO_2 eigenfunction 1 at $y = 0.4De$ g) CO_2 eigenfunction 1 at $y = 0.4De$

b) CO_2 eigenfunction 1 at $y = 2.6De$ e) CO_2 eigenfunction 1 at $y = 2.6De$ h) CO_2 eigenfunction 1 at $y = 2.6De$

c) CO_2 eigenfunction 1 at $y = 5.7De$ f) CO_2 eigenfunction 1 at $y = 5.7De$ i) CO_2 eigenfunction 1 at $y = 5.7De$

Fig. 2 First eigenfunctions of CO_2 at $y = 0.4De$ (a, d, g), $2.6De$ (b, e, h) $5.7De$ (c, f, i) for a–c) $AR = 1$, d–f) $AR = 2$, and g–i) $AR = 3$ jets. Notice the lobes that develop in the corner regions and the ridges that develop along the major sides of the jets.

and topology of the coherent structures in these jets.[43,44] Comparisons of detailed data of these structures with POD results indicate that different vorticity eigenfunctions can be associated with specific vortex orientations. For instance, the first eigenfunction at $y = 2.6De$ (see Fig. 4) appears to capture streamwise vorticity in the form of rib pairs for the square jet and single ribs aligned with corner regions in the rectangular jets. The rib pairs present in the square jet produce larger streamwise vorticity and larger jet spreading in the corner regions of the square jet than for the rectangular jets at $y = 2.6De$, consistent with the spreading seen in the CO_2 eigenfunctions. The second eigenfunction appears to capture portions of the azimuthal vortex ring more strongly than other eigenfunctions, as well as capturing additional streamwise vortex formations, including vortex ring distortion and rib pair coupling in the square jet. The third eigenfunction (not displayed) also captures primarily streamwise vorticity.

Comparisons of the first eigenfunctions of CO_2 and vorticity reveal similar shapes and nonzero spatial extent at each axial location. This is expected because it is vortex-driven convective mixing that dominates in these reactive jets. Highly correlated entrainment and fuel burning rates are expected as the *AR*-dependent coherent structures have an important role in jet spreading, mixing, and combustion.[44]

Axis Switching

Studies have shown that as a rectangular jet spreads, the shape of its cross section can evolve with downstream distance in such a way that the axes of the jet will rotate in ways determined by the jet geometry. As the jet spreads, it will contract in the direction of the major axis and expand in the direction of the minor axis. The cross section will evolve through an intermediate rhomboidal shape where the jet widths are equal in both directions, termed the crossover location. The axes of a square jet rotate 45 deg while those of a rectangular jet rotate 90 deg, interchanging the major and minor axes of the jet. This is denoted as axis switching.[43,44,56] Rectangular jets passively improve mixing through enhanced entrainment due to axis-switching. Axial forcing of these jets is one way to make axis switching more pronounced, by increasing the vortex ring strength and coherence.[43,44]

Table 1 Percentage of information content of each CO_2 and vorticity magnitude eigenfunction presented

Eigenfunction	*AR*	$y = 0.4De$, %	$y = 2.6De$, %	$y = 5.7De$, %
CO_2: 1st	1	95.22	90.08	80.74
	2	95.78	86.11	84.74
	3	97.18	87.32	85.71
Vorticity: 1st	1	92.97	71.94	61.86
	2	92.89	67.73	59.16
	3	93.26	67.29	60.95
Vorticity: 2nd	1	5.78	6.43	5.05
	2	5.76	6.38	5.36
	3	5.69	7.83	5.09

The streamwise location of axis switching increases with aspect ratio. In the present results, axis switching can be seen in several of the eigenfunctions in Fig. 6. The eigenfunctions make axis-switching phenomena more apparent than individual distributions from the ensembles. For the $AR = 1$ jet, the first axis switching occurs at approximately $y = 2.5De$. The 45-deg rotated vortex ring and its influence can be seen in the first eigenfunctions of both vorticity and CO_2. For the $AR = 2$ jet, the first 90-deg axis switching occurs at approximately $5De$ and can be seen in the second eigenfunction of vorticity at $y = 4.8De$ in Fig. 6. The first switching for the $AR = 3$ jet occurs past $6.6De$. At the axial locations studied here,

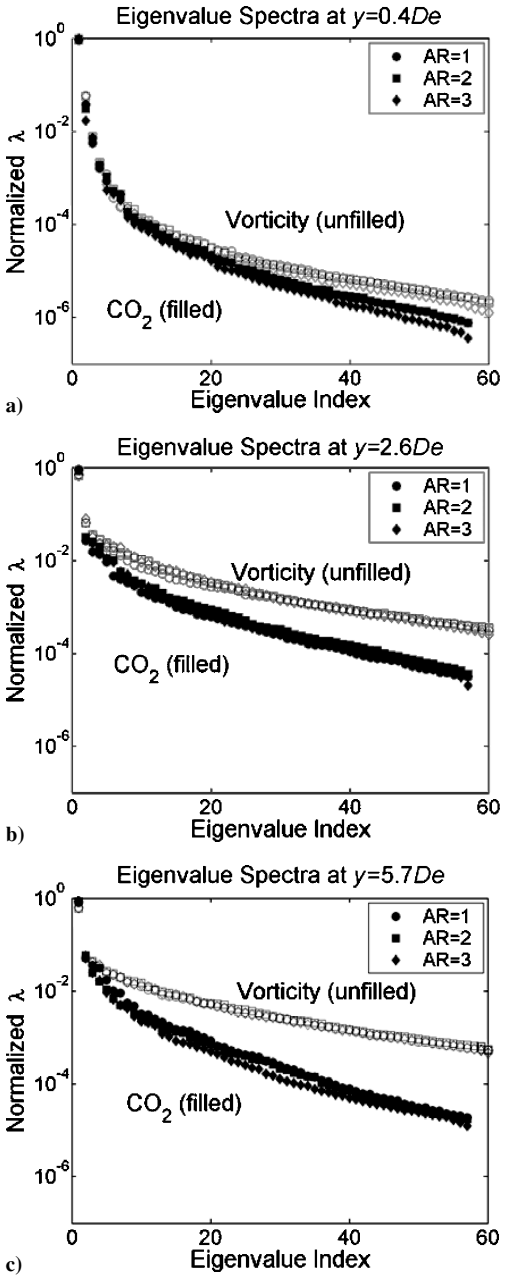

Fig. 3 Eigenvalue spectra for CO_2 and vorticity eigenfunctions at a) $y = 0.4De$, b) $y = 2.6De$, and c) $y = 5.7De$.

it is only possible to see the intermediate rhomboidal jet cross section at the crossover location in the first eigenfunction of vorticity at $y = 6.6De$ for the $AR = 3$ jet. POD analyses were performed at the downstream locations chosen based on expected axis-switching distances in the three jets, determined in previous studies.[43,44,57] The switching distance for the $AR = 1$ jet is expected to be approximately one-half and one-third of the distances for the $AR = 2$ and $AR = 3$ jets, respectively. This expectation is consistent with the results seen in the POD eigenfunctions.

Eigenvalue Spectra and the Potential for Reduced Modeling

Eigenvalue spectra for CO_2 and vorticity magnitude are shown in Fig. 3 for the locations $y = 0.4$, 2.6, and $5.7De$. Near the jet exit, the spectra for both fields drop off rapidly, indicating that the majority of information in each set of eigenfunctions is contained in the first few eigenfunctions. This indicates a strong potential for reduced-order modeling using a small number of eigenfunctions to represent distributions contained in the ensembles of CO_2 and vorticity distributions. As axial distance from the jet increases (moving downstream), the information content of a subset of a fixed number of eigenfunctions decreases in each case, evident in the slower decrease in the eigenvalue spectra. At downstream locations more eigenfunctions are needed to capture the same amount of information that is present in a smaller number of eigenfunctions closer to the jet exit. This is a result of the evolution of the flow through transition to turbulence and breakup of large-scale structures, leading to an increase in complexity as measure by the required number of eigenfunctions necessary to represent the flow. The decrease of information in a given subset of eigenfunctions continues until approximately $y = 4De$, beyond which point the information content of a subset of eigenfunctions remains approximately the same. The eigenfunctions, on the other hand, continue to change. This indicates that the CO_2 and vorticity fields have reached a constant level of complexity as measured by the information content of a fixed number of eigenfunctions.

At all axial locations, the eigenvalue spectra for the three different aspect-ratio jets are approximately the same, indicating that about the same number of eigenfunctions are needed in each jet to capture a given amount of information. Comparing the CO_2 spectra and the vorticity magnitude spectra, it is seen that the information content of a subset of eigenfunctions of CO_2 is greater than the information content of the same number of vorticity eigenfunctions, more significantly as distance from the jet exit is increased. Near the jet exit, CO_2 production is primarily governed by production in regions mixed through large-scale vortex formations, resulting in similar eigenfunctions and eigenvalue spectra for the two fields. Farther downstream, the CO_2 field is more diffuse and uniform as its presence is determined not only by production in mixed regions but also by convective and diffusive transport. Differences are seen in the eigenfunctions as vorticity eigenfunctions contain more small-scale structure than CO_2 eigenfunctions at these downstream locations (compare Figs. 2 and 4), requiring use of additional vorticity eigenfunctions to capture the information in the flow. Hence, reduced-order modeling based on a small number of eigenfunctions might be more feasible for the CO_2 field than for vorticity.

The development of a reduced-order model is dependent on the ability of a limited number of basis functions to capture the flow physics and represent the important flow parameters. The POD eigenfunctions presented here are the most efficient basis set possible for this particular problem. A reduced-order model could be developed through Galerkin projection of the governing equations of the flow onto the basis functions,[18] resulting in a set of ordinary differential equations that describe the flow through the evolution of the associated time coefficients of each basis function. A reduced-order model based on a subset of the most important eigenfunctions would require modeling of the small-scale processes not captured by these eigenfunctions; however, this would be true for any reduced-order model. For control applications, input and output parameters can be represented by an expansion of basis functions and relations between these parameters used to develop a reduced-order model using system identification methods or Galerkin projection of the governing equations. Development of a reduced-order model for control is often system specific and can be highly dependent on the basis set utilized.

Relevant to this study, two-dimensional POD analysis of the flow provides a basis set for use with two-dimensional measurements of combustion parameters for tomographic or other applicable techniques. Measurements in the cross-stream direction allow for the study of axis-switching phenomena present in these jets. In a measurement context, three-dimensional measurements of quantities such as pressures, species concentrations, temperature, emission, etc., are often difficult and costly. One- or two-dimensional measurements are often made on a combustion system at fixed locations. Measurements of these quantities can then be used for feedback control of the system utilizing a reduced-order model based on the measured parameters at these fixed locations.[11,13,25,58,59] CO_2 eigenfunctions could be used to develop a model for CO_2 formation rate, which is proportional to the heat-release rate and hence could be used in combustion instability studies. CO_2 eigenfunctions also can be used for tomographic analysis[28,37] and monitoring of a

a) Vorticity eigenfunction 1 at $y = 0.4De$ d) Vorticity eigenfunction 1 at $y = 0.4De$ g) Vorticity eigenfunction 1 at $y = 0.4De$

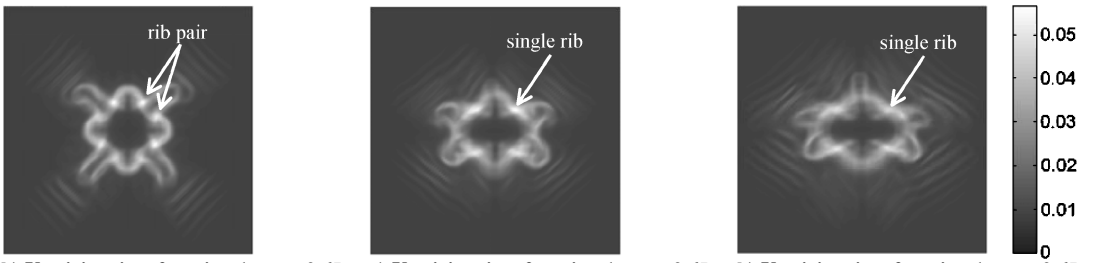

b) Vorticity eigenfunction 1 at $y = 2.6De$ e) Vorticity eigenfunction 1 at $y = 2.6De$ h) Vorticity eigenfunction 1 at $y = 2.6De$

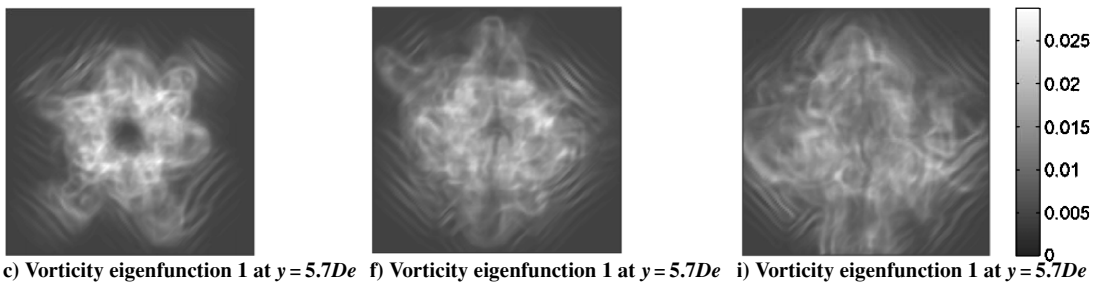

c) Vorticity eigenfunction 1 at $y = 5.7De$ f) Vorticity eigenfunction 1 at $y = 5.7De$ i) Vorticity eigenfunction 1 at $y = 5.7De$

Fig. 4 First eigenfunctions of vorticity at $y = 0.4De$ (a, d, g), $2.6De$ (b, e, h), and $5.7De$ (c, f, i) for a–c) $AR = 1$, d–f) $AR = 2$, and g–i) $AR = 3$ jets.

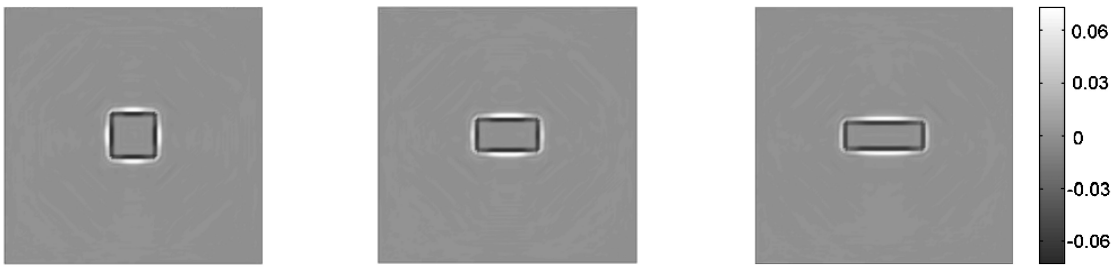

a) Vorticity eigenfunction 2 at $y = 0.4De$ d) Vorticity eigenfunction 2 at $y = 0.4De$ g) Vorticity eigenfunction 2 at $y = 0.4De$

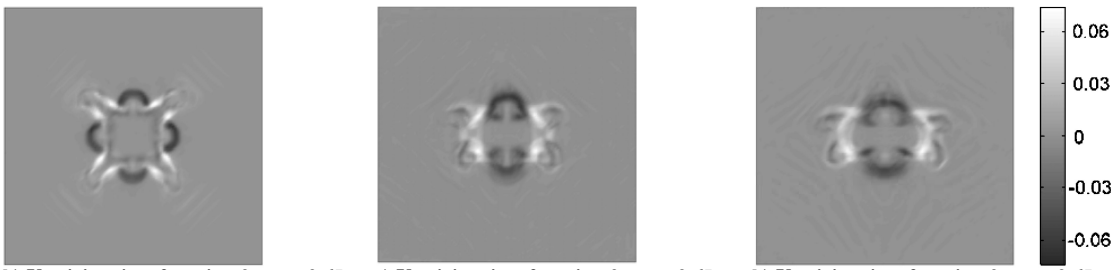

b) Vorticity eigenfunction 2 at $y = 2.6De$ e) Vorticity eigenfunction 2 at $y = 2.6De$ h) Vorticity eigenfunction 2 at $y = 2.6De$

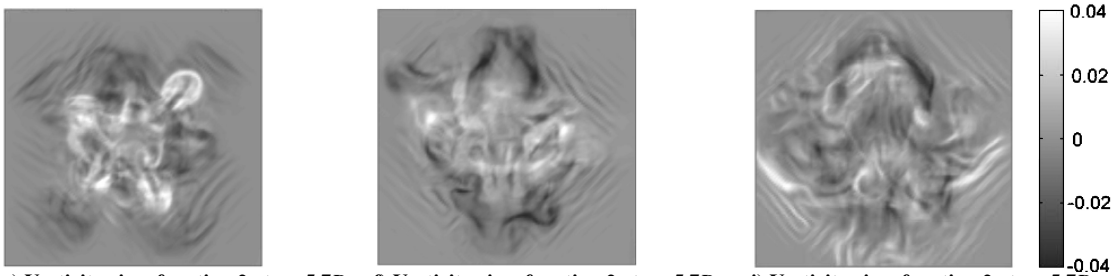

c) Vorticity eigenfunction 2 at $y = 5.7De$ f) Vorticity eigenfunction 2 at $y = 5.7De$ i) Vorticity eigenfunction 2 at $y = 5.7De$

Fig. 5 Second eigenfunctions of vorticity at $y = 0.4De$ (a, d, g), $2.6De$ (b, e, h), and $5.7De$ (c, f, i) for a–c) $AR = 1$, d–f) $AR = 2$, and g–i) $AR = 3$ jets.

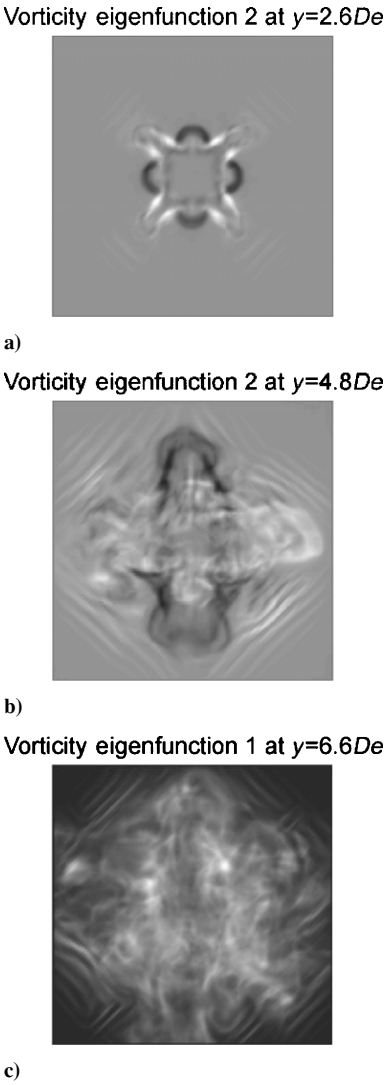

Fig. 6 Vorticity eigenfunctions displaying axis switching in the three jets: a) switching first occurs at $y = 2.6De$ for $AR = 1$, b) switching first occurs at $y = 4.8De$ for $AR = 2$, c) switching occurs past $y = 6.6De$ for $AR = 3$; intermediate rhomboidal shape at crossover is displayed here.

combustion system. Studies have shown that vortex dynamics are linked to sustaining combustion instabilities,[10,14,46] indicating that development of a reduced-order model based on vortex dynamics could be important for use in active combustion control. The results of the POD analysis presented here are representative of the jets under investigation and reflect the flow dynamics evident in the ensemble of distributions from which they were derived. Therefore, the eigenfunctions are specific to each jet and downstream location in this study; nonetheless, they are useful for developing models of these jets for use in combustion control applications where forced jets are of interest as actuators.[3–7]

The information content of subsets of eigenfunctions E_M is quantified in Tables 2 and 3 for different axial locations. Because the eigenvalue spectra for the three jets are approximately the same at each axial location, average values of the information content of the three jets have been used.

A way to examine the representational capabilities of subsets of eigenfunctions is to calculate the best representation of a given distribution in the training set. The best representation of a distribution $n(x, z, t_k)$ using a subset of M eigenfunctions is given by

$$n(x, z, t_k) \approx \hat{n}(x, z, t_k) = \sum_{i=1}^{M} \beta_i(t_k)\phi_i(x, z) \tag{8}$$

where $\hat{n}(x, z, t_k)$is the best representation using the first M eigenfunctions and $\beta_i(t_k)$ is the associated weighting factor for each

Table 2 Comparison of information content of subsets of CO_2 eigenfunctions (average values for the three aspect-ratio jets)

E_M	$y = 0.4De$, %	$y = 2.6De$, %	$y = 5.7De$, %
E_1	96.06	87.84	83.73
E_5	99.81	95.6	95.58
E_{10}	99.94	97.95	98.13

Table 3 Comparison of information content of subsets of vorticity eigenfunctions (average values for the three aspect-ratio jets)

E_M	$y = 0.4De$, %	$y = 2.6De$, %	$y = 5.7De$, %
E_1	93.04	68.99	60.66
E_5	99.78	83.98	76.04
E_{10}	99.91	90.54	84.79

Table 4 Errors in representations of chosen CO_2 and vorticity magnitude distributions using subsets of eigenfunctions are presented

Distribution	M	e_{rms}	e_{abs}	$e_{\max}$
CO_2, $2.6De$	2	0.2894	0.2203	2.9508
	4	0.2030	0.1526	0.6853
	6[a]	**0.1640**	**0.1255**	**0.7915**
	8	0.1450	0.1126	0.7070
	10	0.1256	0.0981	0.6143
	12	0.1196	0.0911	0.5912
Vorticity, $2.6De$	2	0.4516	0.4403	0.8169
	4	0.4469	0.4515	0.8135
	6	0.3009	0.2688	0.3825
	8	0.2717	0.2512	0.9630
	10	**0.2576**	**0.2242**	**0.4230**
	12	0.2517	0.2116	0.4154

[a]Boldfaced values indicate the representations presented in Figs. 7 and 8.

eigenfunction ϕ_i at time t_k. The weighting factors are chosen to minimize the difference between the actual distribution and the best representation of that distribution, that is, to minimize the norm $\|n - \hat{n}\|$ given M eigenfunctions. The weighting factors are calculated by taking the inner product of the actual distribution with each eigenfunction. It is thus possible to reduce the representation problem to order M, where M is the number of eigenfunctions determined to give a sufficiently accurate representation of a distribution. Sirovich suggests defining the representational dimension as the number of eigenfunctions with eigenvalues greater than 1% of the first eigenvalue.[27] An expansion based on these eigenfunctions will capture at least 90% of the total information. For example, based on this concept, 10 vorticity eigenfunctions and six CO_2 eigenfunctions (capturing 91.5% and 97.0%, respectively) are necessary for the $AR = 1$ jet at $y = 2.6De$. The number of eigenfunctions needed for a particular model or representation will most likely be chosen based on the accuracy needed for a given application. Sample representations are presented in Figs. 7 and 8. The associated errors are quantified in Table 4 using the following error measures discussed in Ref. 60.

1) Normalized rms error:

$$e_{\text{rms}} = \frac{\|n(x_i, z_j) - \hat{n}(x_i, z_j)\|_F}{\|n(x_i, z_j) - \bar{n}\|_F} \tag{9}$$

where

$$\bar{n} = \sum_{i=1}^{N_x}\sum_{j=1}^{N_z} \frac{n(x_i, z_j)}{N_x N_z} \tag{10}$$

2) Normalized absolute error:

$$e_{\text{abs}} = \frac{\sum_{i=1}^{N_x}\sum_{j=1}^{N_z} |n(x_i, z_j) - \hat{n}(x_i, z_j)|}{\sum_{i=1}^{N_x}\sum_{j=1}^{N_z} |n(x_i, z_j)|} \tag{11}$$

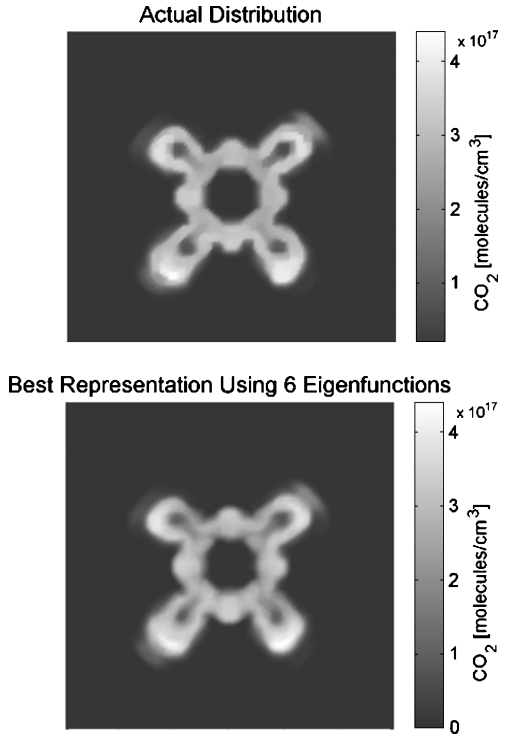

Fig. 7 Representation results using six eigenfunctions of a representative CO_2 distribution in the square jet at $y = 2.6De$.

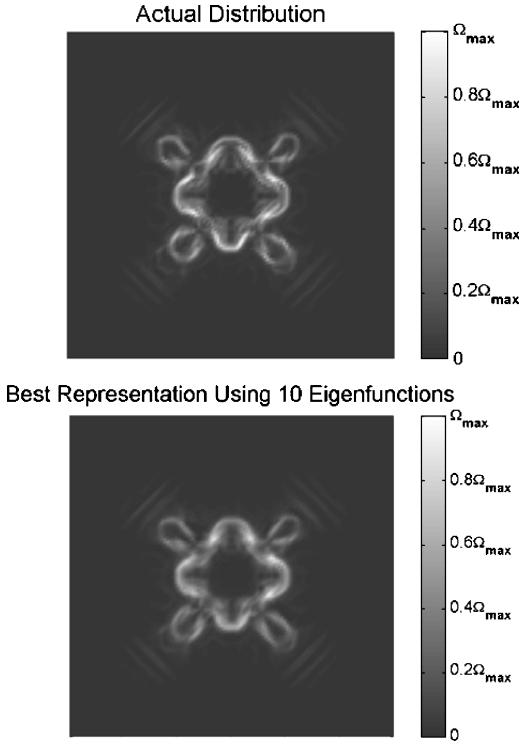

Fig. 8 Representation results using 10 eigenfunctions of a representative vorticity magnitude distribution in the square jet at $y = 2.6De$.

3) Normalized maximum error:

$$e_{\max} = \frac{\max[|n(x_i, z_j) - \hat{n}(x_i, z_j)|]}{n(x_{\max}, z_{\max})} \tag{12}$$

Summary

Proper orthogonal decomposition has been used to analyze ensembles of two-dimensional distributions of concentration and vorticity magnitude in forced reacting rectangular jets of aspect ratios 1–3. The ensembles were constructed at various downstream locations using CO_2 concentration and vorticity magnitude data obtained by computation; they contained 60 and 63 members, respectively. Proper orthogonal decomposition produced sets of eigenfunctions useful for investigating the large-scale features of the flow, and eigenvalues used to evaluate the information content of the eigenfunctions and the potential for reduced-order modeling of these combustion variables using a limited number of basis functions. Although not part of this investigation, spectral analysis of the POD-derived time coefficients could be used to investigate the temporal contributions of individual eigenfunctions and to gain insight into the dynamics of the flow.

Results of proper orthogonal decomposition applied to CO_2 concentration and vorticity magnitude distributions show CO_2 eigenfunctions and vorticity eigenfunctions of similar shapes and nonzero spatial extent, consistent with the understanding that vortex-driven mixing dominates in these jets. The results show similar eigenfunctions for the different aspect-ratio jets at locations near the jet exit. However, the similarity decreases as downstream distance from the jet exit increases. The differences are evident in the different vortex structures that are captured in the rectangular jets and square jet eigenfunctions, for example, single ribs located in corner regions of the rectangular jets as opposed to rib pairs present in the square jet, and result from the inherent differences in the vortex dynamics of these jets. Differences in the extent of the spreading of the CO_2 eigenfunctions between the rectangular and square jets are also displayed, resulting from the different vortex structures just mentioned. The vorticity eigenfunctions can be associated to some extent with different vortex orientations, for example, the first eigenfunction appears more correlated with streamwise vorticity, whereas the second eigenfunction is more correlated with the azimuthal vortex ring. Axis switching is evident in the eigenfunctions at axial locations that are consistent with expectations, for example, axis-switching distances increase with aspect ratio. Although new structures or flow physics have not been revealed through the POD analysis, it is useful in the interpretation of the LES results as it eliminates the need for detailed analysis of many timesteps. Large-scale structures are easily identified in the POD results, and phenomena such as axis switching are readily apparent.

Eigenvalue spectra and eigenfunction information content are examined at various downstream locations. Near the jet exit, the spectra for both CO_2 and vorticity magnitude show that the majority of the information contained in the eigenfunctions is present in the first few eigenfunctions of CO_2 and vorticity, which indicates a good potential for reduced-order modeling at this axial location. However, the complexity of the CO_2 and vorticity eigenfunctions increases as distance from the jet exit increases up to approximately $y = 4De$. This indicates that additional eigenfunctions would be necessary for reduced-order modeling at locations farther downstream, and the potential for reduced-order modeling based on a small set of eigenfunctions at these locations is less than that near the jet exit. After approximately $4De$, evaluation of the eigenfunction information content and the eigenvalue spectra suggests that a constant level of complexity in the flow has been reached. This is evident in the near constant amount of information content contained in a fixed number of eigenfunctions as distance from the jet exit is increased past this location. At each axial location the eigenvalue spectra are approximately the same for the different aspect-ratio jets, indicating that a similar amount of information is contained in a fixed number of eigenfunctions for each of the jets. However, the information content of a fixed number of CO_2 eigenfunctions is greater than the information content of the same number of vorticity eigenfunctions, indicating a greater potential for reduced-order modeling of the CO_2 concentration field. As a result, more vorticity eigenfunctions are needed to accurately represent a vorticity distribution from the ensemble than the number required for a representation of a CO_2 distribution of the same accuracy.

In this paper, we have investigated the results of proper orthogonal decomposition analysis on unsteady, reacting rectangular jets. Through evaluation of the eigenvalue spectra and eigenfunction information content, we have determined that there is a stronger

potential for reduced-order modeling of the CO_2 field than for the vorticity field, although these potentials are approximately the same for the three rectangular jets studied. We have gained physical insight through examination of the resulting eigenfunctions, specifically relating to vortex structures and the development of the CO_2 concentration field through mixing and spreading at locations downstream from the jet exit. Axis-switching phenomena and the influence of vortex dynamics on mixing are also evident in the POD eigenfunctions.

Appendix A: Grid-Resolution Issues

The computational domains used in the original simulations in Ref. 44 had streamwise lengths between 7*De*-10*De* and extended up to 5*De*-10*De* away from the jet axis in the transverse directions. Various grids were used in the original simulations; for $AR = 1$, for example, the number of grid points ranged between $87 \times 112 \times 87$ (spacing 2Δ) to $174 \times 225 \times 174$ (spacing Δ), with most of the simulations typically carried out on computationally convenient grids at the intermediate resolution 1.5Δ; the smallest cell size considered was $\Delta = De/42$ (Refs. 43 and 44). In all cases, the time step used in the temporal integration was determined as a function of the smallest grid spacing based on a fixed Courant number of 0.4. The computational grids used evenly spaced cells in the shear flow region of interest. Geometrical grid stretching in the cross-stream direction outside of the latter region was used to implement the open boundary conditions there.[43] The data used for the POD analysis on the rectangular jets in this investigation were generated at the intermediate resolution with characteristic spacing 1.5Δ. Data sets were obtained from similar simulations of a nonreacting square jet carried out on the finest and coarsest such grids. Because the vortex dynamics and topology of the reacting rectangular and nonreacting square jets are similar and the Reynolds-number regime is the same, the nonreacting square jet simulations are applicable to address grid-resolution issues in what follows.

Because we are dealing here with LES (as opposed to DNS), the meaningful issue to be addressed is convergence of the largest scales of the simulated flow. Figure A1 compares vorticity distributions on streamwise planes passing through the jet axis; run rc40 was carried out on the $174 \times 225 \times 174$ grid with one-half the mesh spacing of the $87 \times 112 \times 87$ rc36 grid; the finest-resolved vorticity data were interpolated onto a grid with the same spacing as the coarsest to generate the frames in Fig. A1. Comparison of snapshots at representative selected times in Fig. A1 indicates that the large-scale features are virtually identical in the first few diameters of streamwise extent, say, up to a transitional location of $y_0 \approx 2.75De$; downstream of which differences are more apparent, reflecting significantly more smaller-scale features captured on the finest grid after transition to turbulence—which also affect the large scales of the simulated flow.

Figures A2 and A3 examine the grid-resolution issues from the perspective of POD analysis. Analysis is based on the available vorticity simulation data from runs rc40 and rc36 at 10 equally spaced time steps, over a time interval spanning two forcing periods—significantly less than that used in the POD analysis just presented (60 samplings over six forcing periods). A large number of distributions is desirable for POD analysis, and additional grids would allow for more comprehensive convergence studies; however, the production of numerous distributions on different LES grids is computationally intensive, and thus we have chosen to use preexisting simulation data for the present grid-resolution studies.[43–45]

POD analysis is useful for investigating grid-resolution issues in an unsteady process, as differences in the flow resulting from changes in the simulation grid will alter both the resulting eigenfunctions and eigenvalue spectra. The specific nature of the eigenfunctions makes them useful as a mechanism for determining the adequacy of LES resolution through evaluation of the small-scale information captured in the eigenfunctions and the associated eigenvalue spectra. Changes in the eigenvalue spectra caused by differing amounts of small-scale information captured on the different grids

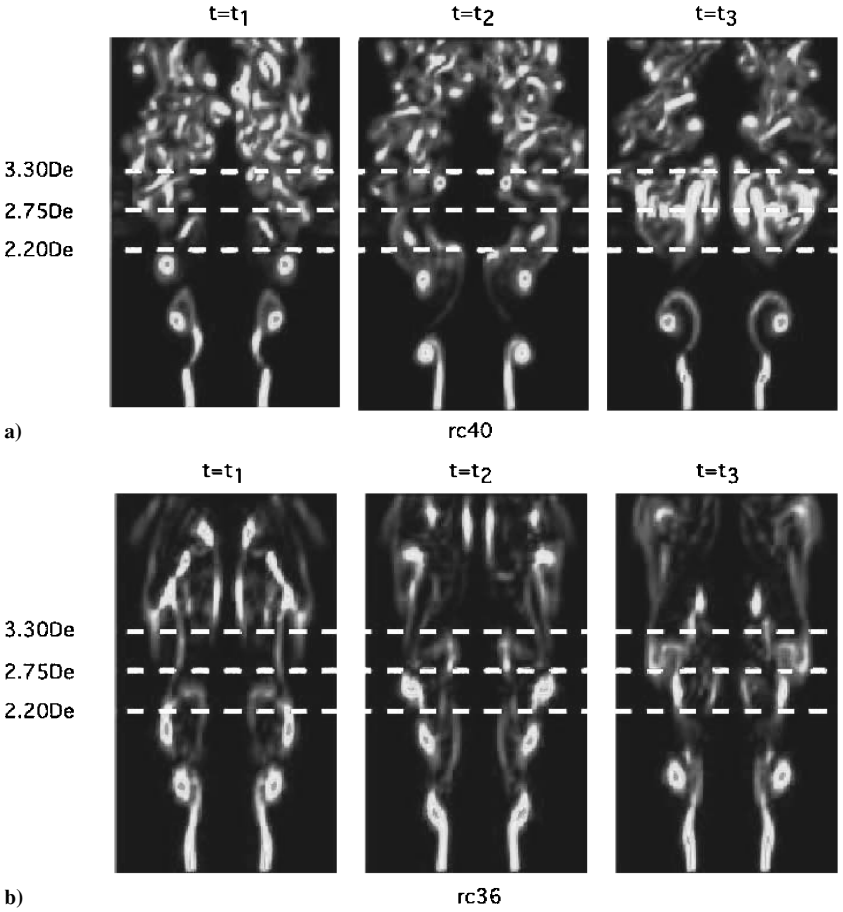

Fig. A1 Vorticity distributions on streamwise planes passing through the jet axis for a) run rc40 and b) run rc36.

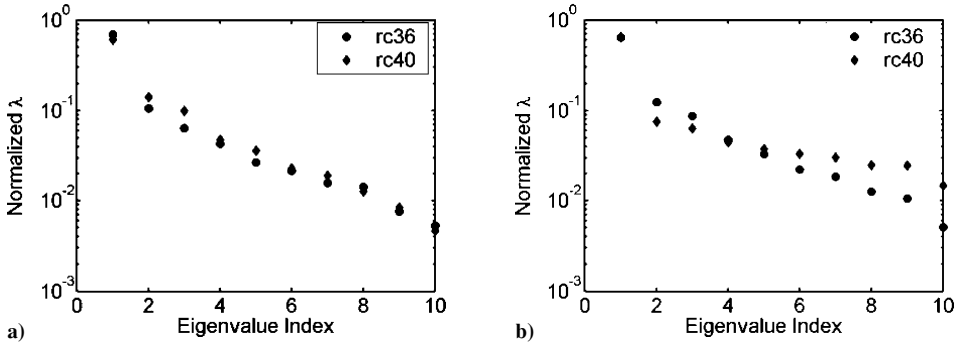

Fig. A2 Normalized eigenvalue spectra at a) $y_1 = 2.2De$ and b) $y_2 = 3.3De$.

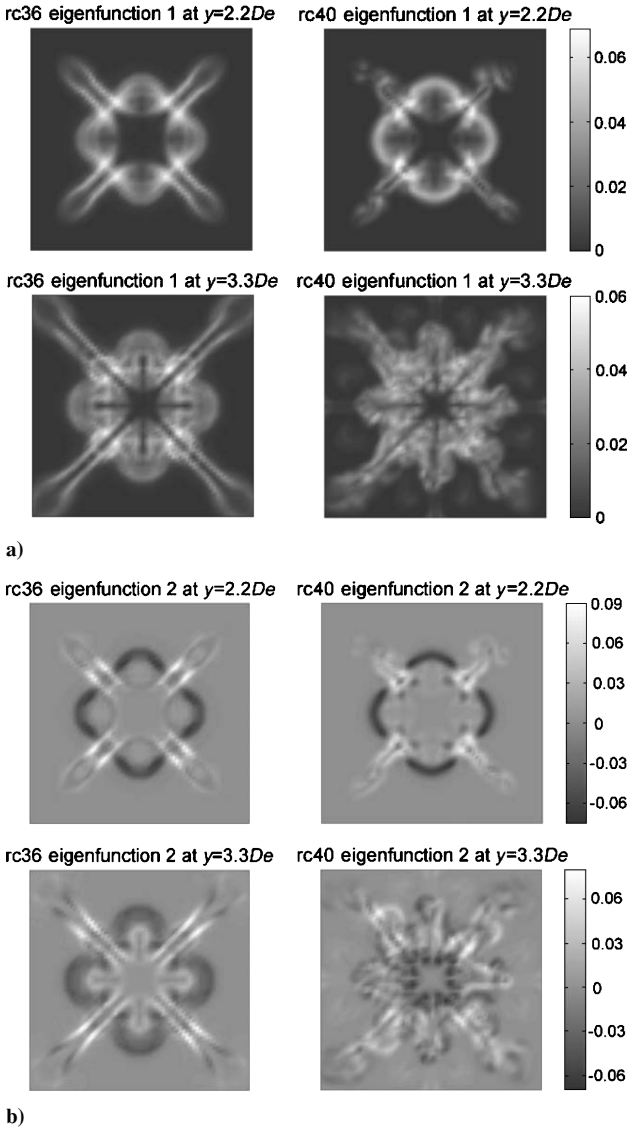

Fig. A3 Comparison of eigenfunctions from re36 and re40 jet simulations: a) first eigenfunctions of vorticity for rc36 jet (left) and rc40 jet (right) at $y_1 = 2.2De$ (top) and $y_2 = 3.3De$ (bottom); and b) second eigenfunctions of vorticity for rc36 and rc40 jets at $y_1 = 2.2De$ (top) and $y_2 = 3.3De$ (bottom).

are useful in evaluating grid resolution. The relevant quantity to be computed is the amount of information contained in a subset of eigenfunctions as deduced from the eigenvalue spectra. By comparison of a subset of eigenfunctions resulting from POD analysis of different grid resolutions, if the eigenvalue spectra are suitably similar for the different grids, one can determine a measure of grid-resolution suitability based on the amount of information contained in the subset of eigenfunctions.

Figure A2 compares the normalized eigenvalue spectra at two relevant streamwise locations, $y_1 = 2.2De < y_0$ and $y_2 = 3.3De > y_0$. By design, y_1 and y_2 were chosen to straddle the transitional location $y = y_0$. The two eigenvalue spectra compare favorably at $y = y_1$, but somewhat less favorably at $y = y_2$, especially at higher index number. In Fig. A3, large-scale coherent structures are seen in the eigenfunctions resulting from the coarsely gridded rc36 simulation. The lack of small-scale information in the rc36 eigenfunctions results in a fast decline in the eigenvalue spectra at both downstream locations. This simulation is capable of capturing the large-scale vorticity formations but is unable to capture the smallest scale coherent structures, the high intensity "worm" vortices as described in Ref. 44. The finely gridded rc40 simulation is able to resolve the worm vortices and thus captures more small-scale information in the flow. These small-scale structures can be seen in the resulting eigenfunctions in Fig. A3 and cause the flattening of the rc40 eigenvalue spectrum as information is shifted from the lower to the higher eigenfunctions, seen in Fig. A2 at $y_2 = 3.3De$. At the downstream location y_1, the eigenvalue spectra for the two simulations are similar, and a subset of the first four eigenfunctions captures approximately 90% of the information in the flow for each simulation. Farther downstream at y_2, the same subset of eigenfunctions captures approximately 90% of the information in the rc36 simulation but only 83.5% of the information in the rc40 simulation. Comparison of the information content on additional grids would allow for further evaluation of grid resolution; the convergence features are likely to depend on ensemble specifics (e.g., number of samplings involved, downstream location, etc.).

Appendix B: Proper-Orthogonal-Decomposition Matrix Formulation

The matrix formulation of the POD is presented following the formulation in Ref. 27. As stated in the main text, consider an ensemble of distributions $\{n\}$. An individual distribution is a scalar function of position and time $n(x, z, t_k)$ and can be written as $\boldsymbol{n}^k(\boldsymbol{x})$. Consider $\boldsymbol{C}$ as a matrix containing the ensemble distributions $\{\boldsymbol{n}^k(\boldsymbol{x})\}$ such that each member of the ensemble is contained in a row of $\boldsymbol{C}$ of length $N_p = N_x \times N_z$ resulting in a $N_t \times N_p$ matrix:

$$\boldsymbol{C} = \begin{bmatrix} n^1(\boldsymbol{x}) \\ \vdots \\ n^{N_t}(\boldsymbol{x}) \end{bmatrix} \tag{B1}$$

We seek a system of orthonormal functions $\{\phi^k(\boldsymbol{x})\}$ such that

$$(\phi^k(\boldsymbol{x}), \phi^l(\boldsymbol{x})) = \int_\Omega \phi^k(\boldsymbol{x})\phi^l(\boldsymbol{x})\,\mathrm{d}\boldsymbol{x} = \delta_{\mathrm{kl}} \tag{B2}$$

Consider a $N_t \times N_p$ matrix $\boldsymbol{\Phi}$ such that each row is a vector denoting a member of the set $\{\phi^k(\boldsymbol{x})\}$:

$$\boldsymbol{\Phi} = \begin{bmatrix} \phi^1(\boldsymbol{x}) \\ \vdots \\ \phi^{N_t}(\boldsymbol{x}) \end{bmatrix} \tag{B3}$$

The set $\{\phi\}$ can then be normalized according to $\Phi \boldsymbol{G} \Phi^T = \boldsymbol{I}$. $\boldsymbol{G}$ is an integration matrix used to approximate the spatial integration of a function in the x and z directions using the trapezoidal rule. The members of $\{\phi\}$ are chosen such that

$$\lambda_k = \langle (\phi^k, n)^2 \rangle = \frac{1}{N_t} \sum_{m=1}^{N_t} (\phi^k, n^m)^2 \tag{B4}$$

is a maximum.

The method of snapshots calculates ϕ as an admixture of distributions, that is, "snapshots" in the ensemble.[27]

$$\phi = \sum_{k=1}^{N_t} a_k n^k \tag{B5}$$

A two-time correlation matrix $\boldsymbol{D}$ is formulated according to

$$D_{jk} = \frac{1}{N_t} (n^j(\boldsymbol{x}), \boldsymbol{n}^k(\boldsymbol{x})) = \frac{1}{N_t} \int_\Omega n^j(\boldsymbol{x}) \boldsymbol{n}^k(\boldsymbol{x}) \, \mathrm{d}\boldsymbol{x} \tag{B6}$$

leading to the matrix equation $\boldsymbol{D} = (1/N_t) \boldsymbol{C} \boldsymbol{G} \boldsymbol{C}^T$, where $\boldsymbol{D}$ is a $N_t \times N_t$ matrix. The coefficients $\{a_k\}$ are determined through solution of the eigenvalue problem

$$\sum_{k=1}^{N_t} D_{jk} a_k = \lambda a_j \tag{B7}$$

This can be written in matrix form as $\boldsymbol{D}\boldsymbol{A} = \boldsymbol{\Lambda}\boldsymbol{A}$, where $\boldsymbol{A}$ is a $N_t \times N_t$ matrix, each row of which contains the time coefficients for all eigenfunctions at a time step and $\boldsymbol{\Lambda}$ is a diagonal $N_t \times N_t$ matrix containing the eigenvalues. This is the resulting eigenvalue problem presented in the main text.

Acknowledgment

This work was supported by the Office of Naval Research under Contract N00014-99-1-0447.

References

[1]Gutmark, E., and Grinstein, F., "Flow Control with Noncircular Jets," *Annual Review of Fluid Mechanics*, Vol. 31, 1999, pp. 239–272.

[2]Gutmark, E., Parr, T., Wilson, K., and Schadow, K., "Active Control in Combustion Systems with Vortices," *Proceedings of the 1995 IEEE Conference on Control Applications,* Inst. of Electrical and Electronics Engineers, New York, 1995, pp. 679–684.

[3]Hathout, J., Fleifil, A., Annaswamy, A., and Ghoniem, A., "Role of Actuation in Combustion Control," *Proceedings of the 1999 IEEE International Conference on Control Applications,* Inst. of Electrical and Electronics Engineers, New York, 1999, pp. 213–218.

[4]Hathout, J. P., Fleifil, M., Annaswamy, A. M., and Ghoniem, A. F., "Heat Release Actuation for Control of Mixture-Inhomogeneity-Driven Combustion Instability," *Proceedings of the Combustion Institute*, Vol. 28, Combustion Inst., Pittsburgh, PA, 2000, pp. 721–730.

[5]Murugappan, S., Gutmark, E. J., Acharya, S., and Krstic, M., "Extremum-Seeking Adaptive Controller for Swirl-Stabilized Spray Combustion," *Proceedings of the Combustion Institute*, Vol. 28, Combustion Inst., Pittsburgh, PA, 2000, pp. 731–737.

[6]Lee, J. G., Kim, K., and Santavicca, D., "Effect of Injection Location on the Effectiveness of Active Control System Using Secondary Fuel Injection," *Proceedings of the Combustion Institute*, Vol. 28, Combustion Inst., Pittsburgh, PA, 2000, pp. 739–746.

[7]Johnson, C., Neumeier, Y., Lieuwen, T., and Zinn, B., "Experimental Determination of the Stability Margin of a Combustor Using Exhaust Flow and Fuel Injection Rate Modulations," *Proceedings of the Combustion Institute*, Vol. 28, Combustion Inst., Pittsburgh, PA, 2000, pp. 757–763.

[8]Candel, S., "Combustion Dynamics and Control: Progress and Challenges," *Proceedings of the Combustion Institute*, Vol. 29, Combustion Inst., Pittsburgh, PA, 2002, pp. 1–28.

[9]Ghoniem, A. F., Annaswamy, A., Wee, D., Yi, T., and Park, S., "Shear Flow-Driven Combustion Instability: Evidence, Simulation, and Modeling," *Proceedings of the Combustion Institute*, Vol. 29, Combustion Inst., Pittsburgh, PA, 2002, pp. 53–60.

[10]Paschereit, C. O., and Gutmark, E. J., "Enhanced Performance of a Gas-Turbine Combustor Using Miniature Vortex Generators," *Proceedings of the Combustion Institute*, Vol. 29, Combustion Inst., Pittsburgh, PA, 2002, pp. 123–129.

[11]Park, S., Wachsman, A., Annaswamy, A., Ghoniem, A. F., Pang, B., and Yu, K. H., "Experimental Study of POD-Based Control for Combustion Instability Using a Linear Photodiode Array," AIAA Paper 2004-0639, Jan. 2004.

[12]Hathout, J. P., Annaswamy, A., Fleifil, M., and Ghoniem, A. F., "A Model-Based Active Control Design for Thermoacoustic Instability," *Combustion Science and Technology*, Vol. 132, Nos. 1–6, 1998, pp. 99–138.

[13]Billoud, G., Galland, M. A., Huu, C. H., and Candel, C., "Adaptive Active Control of Combustion Instabilities," *Combustion Science and Technology*, Vol. 81, Nos. 4–6, 1992, pp. 257–283.

[14]Fureby, C., "A Computational Study of Combustion Instabilities due to Vortex Shedding," *Proceedings of the Combustion Institute*, Vol. 28, Combustion Inst., Pittsburgh, PA, 2000, pp. 783–791.

[15]Annaswamy, A. M., and Ghoniem, A. F., "Active Control in Combustion Systems," *IEEE Control Systems Magazine*, Vol. 15, No. 6, 1995, pp. 49–63.

[16]Smaoui, N., "Linear Versus Nonlinear Dimensionality Reduction of High-Dimensional Dynamical Systems," *SIAM Journal on Scientific Computing*, Vol. 25, No. 6, 2004, pp. 2107–2125.

[17]Norman, D. E., "Chemically Reacting Fluid Flows: Weak Solutions and Global Attractors," *Journal of Differential Equations*, Vol. 152, No. 1, 1999, pp. 75–135.

[18]Holmes, P., Lumley, J., and Berkooz, G., *Turbulence, Coherent Structures, Dynamical Systems and Symmetry*, Cambridge Univ. Press, New York, 1996, Chap. 3.

[19]Graham, W. R., Peraire, J., and Tang, K. Y., "Optimal Control of Vortex Shedding Using Low Order Models. Part I—Open-Loop Model Development," *International Journal for Numerical Methods in Engineering*, Vol. 44, No. 7, 1999, pp. 945–972.

[20]Baker, J., and Christofides, P. D., "Finite-Dimensional Approximation and Control of Non-Linear Parabolic PDE Systems," *International Journal of Control*, Vol. 73, No. 5, 2000, pp. 439–456.

[21]Ravindran, S. S., "A Reduced-Order Approach for Optimal Control of Fluids Using Proper Orthogonal Decomposition," *International Journal for Numerical Methods in Fluids*, Vol. 34, No. 5, 2000, pp. 425–448.

[22]Zheng, D., Hoo, K. A., and Piovoso, M. J., "Low-Order Model Identification of Distributed Parameter Systems by a Combination of Singular Value Decomposition and the Karhunen–Loeve Expansion," *Industrial and Engineering Chemistry Research*, Vol. 41, No. 6, 2002, pp. 1545–1556.

[23]Fogleman, M., Lumley, J., Rempfer, D., and Haworth, D., "Application of the Proper Orthogonal Decomposition to Datasets of Internal Combustion Engine Flows," *Journal of Turbulence*, Vol. 5, Art. No. 023, 2004.

[24]Gillies, E. A., "Low-Dimensional Control of the Circular Cylinder Wake," *Journal of Fluid Mechanics*, Vol. 371, 1998, pp. 157–178.

[25]Annaswamy, A., Choi, J. J., Sahoo, D., Alvi, F. S., and Lou, H., "Active Closed-Loop Control of Supersonic Impinging Jet Flows Using POD Models," *Proceedings of the 41st IEEE Conference on Decision and Control*, Inst. of Electrical and Electronics Engineers, New York, 2002, pp. 3294–3299.

[26]Berkooz, G., Holmes, P., and Lumley, J. L., "The Proper Orthogonal Decomposition in the Analysis of Turbulent Flows," *Annual Review of Fluid Mechanics*, Vol. 25, 1993, pp. 539–575.

[27]Sirovich, L., and Emerson, R., "Management and Analysis of Large Scientific Datasets," *International Journal of Supercomputer Applications,* Vol. 6, No. 1, 1992, pp. 50–68.

[28]Tornianen, E., "Tomographic Reconstruction Using a Karhunen–Loeve Basis," Ph.D. Dissertation, Sibley School of Mechanical and Aerospace Engineering, Cornell Univ., Ithaca, NY, May 2000.

[29]Lumley, J., "The Structure of Inhomogeneous Turbulent Flows," *Atmospheric Turbulence and Radio Wave Propagation*, Nauka, Moscow, 1967, pp. 166–178.

[30]Gunes, H., "Low-Dimensional Modeling of Non-Isothermal Twin-Jet Flow," *International Communications in Heat and Mass Transfer*, Vol. 29, No. 1, 2002, pp. 77–86.

[31]Frouzakis, C., Kevrekidis, Y., Lee, J., Boulouchos, K., and Alonso, A., "Proper Orthogonal Decomposition of Direct Numerical Simulation Data: Data Reduction and Observer Construction," *Proceedings of the Combustion Institute*, Vol. 28, Combustion Inst., Pittsburgh, PA, 2000, pp. 75–81.

[32]Bernero, S., and Fiedler, H., "Application of Particle Image Velocimetry and Proper Orthogonal Decomposition to the Study of a Jet in a Counterflow," *Experiments in Fluids*, Vol. 29, No. 7, 2000, pp. S274–S281.

[33]Patte-Rouland, B., Lalizel, G., Moreau, J., and Rouland, E., "Flow Analysis of an Annular Jet by Particle Image Velocimetry and Proper Orthogonal Decomposition," *Measurement Science and Technology*, Vol. 12, No. 9, 2001, pp. 1401–1412.

[34]Citriniti, J., and George, W., "Reconstruction of the Global Velocity Field in the Axisymmetric Mixing Layer Utilizing the Proper Orthogonal Decomposition," *Journal of Fluid Mechanics*, Vol. 418, 2000, pp. 137–166.

[35]Faghani, D., Sevrain, A., and Boisson, H., "Physical Eddy Recovery Through Bi-Orthogonal Decomposition in an Acoustically Forced Plane Jet," *Flow, Turbulence, and Combustion*, Vol. 62, No. 1, 1999, pp. 69–88.

[36]Yilmaz, T., and Kodal, A., "An Investigation of Forced Structures in Turbulent Jet Flows," *Experiments in Fluids*, Vol. 29, No. 6, 2000, pp. 564–572.

[37]Tornianen, E., Hinz, A., and Gouldin, F., "Tomographic Analysis of Unsteady Reacting Flows: Numerical Investigation," *AIAA Journal*, Vol. 36, No. 7, 1998, pp. 1270–1278.

[38]Sirovich, L., Kirby, M., and Winter, M., "An Eigenfunction Approach to Large Scale Transitional Structures in Jet Flow," *Physics of Fluids A*, Vol. 2, No. 2, 1990, pp. 127–136.

[39]Pelliccia-Kraft, J., and Watt, D., "Visualization of Coherent Structure in Scalar Fields of Unsteady Jet Flows with Interferometric Tomography and Proper Orthogonal Decomposition," *Experiments in Fluids*, Vol. 30, No. 6, 2001, pp. 633–644.

[40]Winter, M., Barber, T., Everson, R., and Sirovich, L., "Eigenfunction Analysis of Turbulent Mixing Phenomena," *AIAA Journal*, Vol. 30, No. 7, 1992, pp. 1681–1688.

[41]Aubry, N., Holmes, P., Lumley, J., and Stone, E., "The Dynamics of Coherent Structures in the Wall Region of a Turbulent Boundary Layer," *Journal of Fluid Mechanics*, Vol. 192, 1988, pp. 115–173.

[42]Moehlis, J., Smith, T. R., Holmes, P., and Faisst, H., "Models for Turbulent Plane Couette Flow Using the Proper Orthogonal Decomposition," *Physics of Fluids*, Vol. 14, No. 7, 2002, pp. 2493–2507.

[43]Grinstein, F., "Coherent Structure Dynamics and Transition to Turbulence in Rectangular Jet Systems," AIAA Paper 99-3506, June 1999.

[44]Grinstein, F., "Vortex Dynamics and Entrainment in Rectangular Free Jets," *Journal of Fluid Mechanics*, Vol. 437, 2001, pp. 69–101.

[45]Grinstein, F. F., and DeVore, C. R., "Dynamics of Coherent Structures and Transition to Turbulence in Free Square Jets," *Physics of Fluids*, Vol. 8, No. 5, 1996, pp. 1237–1251.

[46]Pang, B., Yu, K. H., Park, S., Wachsman, A., Annaswamy, A. M., and Ghoniem, A. F., "Characterization and Control of Vortex Dynamics in an Unstable Dump Combustor," AIAA Paper 2004-1162, Jan. 2004.

[47]Grinstein, F., and Kailasanath, K., "Exothermicity and Three-Dimensional Effects in Unsteady Propane Square Jets," *26th International Symposium on Combustion,* Combustion Inst., Pittsburgh, PA, 1996, pp. 91–96.

[48]Fureby, C., and Grinstein, F. F., "Monotonically Integrated Large Eddy Simulation of Free Shear Flows," *AIAA Journal*, Vol. 37, No. 5, 1999, pp. 544–556.

[49]Grinstein, F. F., and Guirguis, R. H., "Effective Viscosity in the Simulation of Spatially Evolving Shear Flows with Monotonic FCT Models," *Journal of Computational Physics*, Vol. 101, No. 1, 1992, pp. 165–175.

[50]Grinstein, F. F., and Kailasanath, K., "Chemical Energy Release and Dynamics of Transitional, Reactive Shear Flows," *Physics of Fluids A*, Vol. 4, No. 10, 1992, pp. 2207–2221.

[51]Fureby, C., and Grinstein, F. F., "Large Eddy Simulation of High-Reynolds-Number Free and Wall-Bounded Flows," *Journal of Computational Physics*, Vol. 181, No. 1, 2002, pp. 68–97.

[52]Grinstein, F. F., and Fureby, C., "From Canonical to Complex Flows: Recent Progress on Monotonically Integrated LES," *Computing in Science and Engineering*, Vol. 6, No. 2, 2004, pp. 37–49.

[53]Westbrook, C., and Dryer, F., "Simplified Reaction Mechanisms for the Oxidation of Hydrocarbon Fuels in Flames," *Combustion Science and Technology*, Vol. 27, No. 1–2, 1981, pp. 31–43.

[54]Peters, N., *Turbulent Combustion*, Cambridge Univ. Press, Cambridge, England, U.K., 2000, Chap. 1.

[55]Williams, F. A., *Combustion Theory*, Benjamin/Cummings, Menlo Park, CA, 1985.

[56]Zaman, K., "Axis Switching and Spreading of an Asymmetric Jet: the Role of Coherent Structure Dynamics," *Journal of Fluid Mechanics*, Vol. 316, 1996, pp. 1–27.

[57]Grinstein, F. F., "Self-induced Vortex Ring Dynamics in Subsonic Rectangular Jets," *Physics of Fluids*, Vol. 7, No. 10, 1995, pp. 2519–2521.

[58]Dunstan, W. J., Bitmead, R. R., and Savaresi, S. M., "Fitting Nonlinear Low-Order Models for Combustion Instability Control," *Control Engineering Practice*, Vol. 9, No. 12, 2001, pp. 1301–1317.

[59]Furlong, E. R., Baer, D. S., and Hanson, R. K., "Real-Time Adaptive Combustion Control Using Diode-Laser Absorption Sensors," *Twenty-Seventh Symposium (International) on Combustion*, Combustion Inst., Pittsburgh, PA, 1998, pp. 103–111.

[60]Verhoeven, D., "Limited-Data Computed Tomography Algorithms for the Physical Sciences," *Applied Optics*, Vol. 32, No. 20, 1993, pp. 3736–3754.

J. Bellan
Associate Editor